

## 2 Optics of the Human Eye

*In all ophthalmic and optometric devices to be presented, the eye is an essential part of the entire optical system. Because of this, the functional principles of these devices cannot be fully understood without an understanding of basic optics of the human eye. In this chapter, we will see that the eye can be described in a similar way as other optical systems. This finding is very important for further discussions in this book, so that this chapter serves as a basic reference.*

The anatomy of the human eye is readily comparable to the design of a photo camera (Figure 2.1). We can thus identify the iris as an aperture stop (Section 2.1.1), that the cornea and eye lens form the objective lens (Section 2.1.4), that the retina is a photo sensor, and that the brain acts as a very sophisticated image processing computer with intelligent algorithms. In contrast to a photo camera, the eye is *not* a centered optical system as its refractive components and aperture stop are not centered at a common optical axis (Section 2.1.3). The performance of the “light sensors” are also different for the photo camera and the human eye. The resolution of the photo camera’s detector is equal for the whole area, whereas the retinal resolution is inhomogeneous (Section 2.1.5). In the central part of the retina, the resolution is high and decreases at the margins.

### 2.1 Optical Imaging

When light is incident to the eye, first of all it enters the cornea. As our eyes are usually surrounded by air, the refractive power (Section A.1.2.1) at the air–cornea interface<sup>1)</sup> is as high as 42 diopters (D). According to the Fresnel<sup>2)</sup> equation (A5), the transmittance of the air–cornea interface is 98%. However, this value does not take scattering (Section 9.2) and absorption (Section 9.1) of the ocular media into

- 1) Strictly speaking, we have to consider the interface between air and the tear film (Section 1.1). However, the refractive indices of the tear film and the corneal layers are very similar. Thus, for the following discussions, we will regard the tear film as being a part of the cornea.
- 2) Augustin Fresnel (1788–1827).

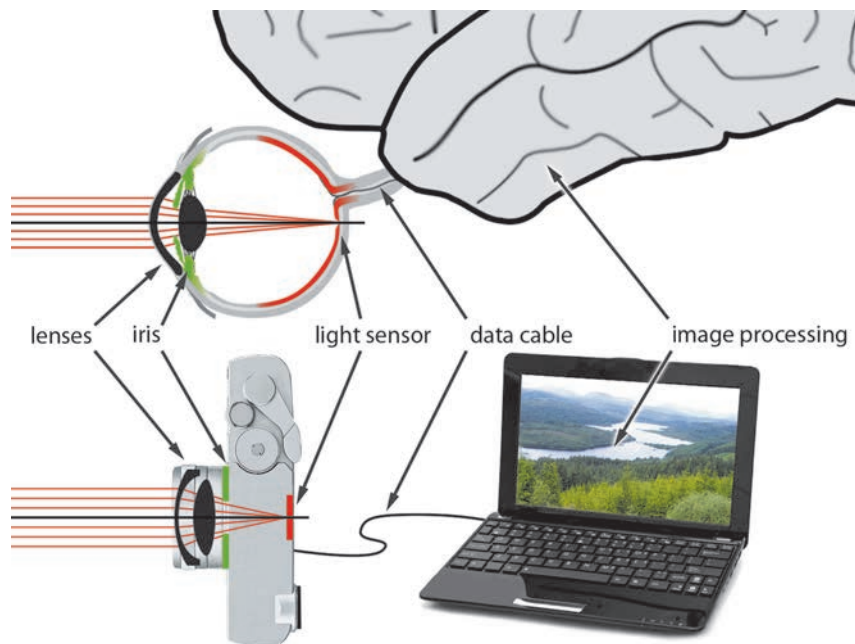


**Figure 2.1** Comparison of human eye and photo camera. The optical system of the photo camera is reduced to the most necessary components. Usually, the arrangement is much more complicated since optical aberrations (Section A.1.7) have to be corrected.

account. Nevertheless, healthy corneal tissue is remarkably transparent. This is due to the ordered collagen fibrils<sup>3)</sup> which are weak scatterers, as their radius is much smaller than the wavelength of visible light (fibril diameter: 25–35 nm; wavelength of visible light: 380–780 nm). In addition, the spatial distribution of fibrils reduces scattering because of destructive interference (Section A.2.3).

After the incident light rays have been refracted (Section A.1.1) by the cornea, they travel through the anterior chamber and cross the iris. For the eye as an optical system, the iris forms an aperture stop with a variable inner diameter (Figure 2.1). It limits the maximum acceptance angle, that is, the so-called *visual field*, for incident light rays to about  $105^\circ$ . On the nasal side, this angle is further reduced to  $60^\circ$  by the nose. For an iris diameter of 8 mm (scotopic vision), the eye has a maximum numerical aperture (Section A.1.4) of about 0.23 [1]. For an iris diameter of 3 mm, the numerical aperture reduces to 0.1.

When the light rays have passed the iris, they travel through the posterior chamber and enter the eye lens. The shape of the eye lens and thus its refractive power can be adjusted depending on the distance of the object being fixated. The lens consists of multiple shells which are stacked layer-by-layer. Each shell has a different refractive index, where a maximum refractive index of 1.42 is found in the core.

3) The human corneal stroma is composed of stacked lamellae. Within each lamella, collagen fibrils run parallel to each other and show a regular spacing (Section 1.1).

Behind the lens, light passes through the vitreous and is eventually “detected” by the retina. The image formed on the retina is inverted, that is, upside down, which is analogous to the imaging of a single lens (Figure A.6). Another inversion process happens in the brain, which results in the correct visual perception of our environment.

### 2.1.1

#### Entrance and Exit Pupils

In ophthalmology and optometry, the term “pupil” is often referred to as the hole of the iris (iris aperture). But technically, the iris is actually an aperture stop (Section A.1.4).<sup>4)</sup> The cornea forms an image of this aperture stop which is in optical terms the entrance pupil of the eye. The exit pupil of the eye is the image of the same aperture stop formed by the eye lens.

As shown in Figure 2.2, we follow the paths of a marginal ray and the chief ray to determine the location and diameter of the entrance and exit pupils. The optical design of the eye has been simplified in this scheme, because we assume that the iris is centered on an optical axis. The chief ray emanates from the outermost off-axis point  $O_1$  of the focused object. It is then refracted by the cornea, crosses the center of the iris, and is again refracted by the eye lens. Eventually, the chief ray hits the retina at point  $I'_1$ . As explained in Section A.1.4, the extensions of the chief ray define the positions of the pupil centers on the optical axis. The detailed view in Figure 2.2b shows the resulting pupil centers, E (entrance pupil) and E' (exit pupil), relative to the ocular parts. The optical design in this figure is not to scale, but reveals correctly that the entrance pupil is larger and in front of the iris.

The marginal ray emanates from an on-axis object point  $O_0$  and grazes the inner edge of the iris. When we extend the object- and image-side parts of the marginal ray to the pupil planes, we obtain the inner diameters of the entrance and exit pupils, respectively.

We can now use the chief ray to determine the image size on the retina. In paraxial approximation (Section A.1.2), the absolute value of the image size follows as<sup>5)</sup> (Figure 2.2):

$$|h'_1| = \varphi' \overline{E'I'_0}. \quad (2.1)$$

The overbar in (2.1) symbolizes the length between the points.<sup>6)</sup> The iris of each human eye is decentered nasally by about 0.5 mm relative to the optical axis (formed by cornea and eye lens). In contrast to centered optical systems, the angles  $\varphi$  and  $\varphi'$  are *not* equal, but it can be shown that the relation  $\varphi'/\varphi = m$  is constant<sup>7)</sup>. With

- |   |   |
|---|---|
| <p>4) In a very crude approximation, iris and entrance pupil coincide.</p> <p>5) Throughout this book, primed variables describe optical design parameters and points within the image space, that is, between the first refracting surface and the</p> | <p>image (see also Section A.1). Unprimed variables are used for object space quantities.</p> <p>6) For example, <math>\overline{E'I'_0}</math> stands for the distance between the center of the exit pupil E' and the on-axis image point <math>I'_0</math>.</p> <p>7) However, <math>m</math> depends on the state of accommodation (Section 2.1.4).</p> |
|---|---|

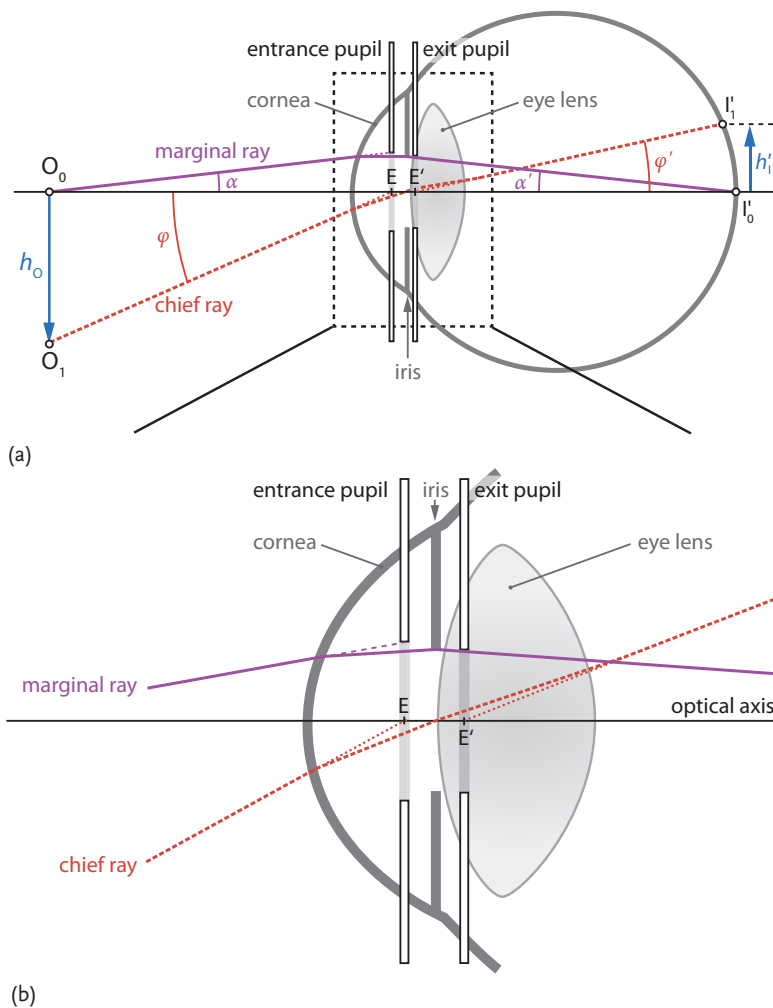


**Figure 2.2** Location of entrance and exit pupils of the human eye. The indication of parameters is comparable to Figure A.13. (a) Path of the chief ray which starts at the outermost point  $O_1$  of the object and passes through the center of the iris. The extensions of the chief ray on the object and image side define the centers of the entrance and exit pupils, respectively.  $E$  is the center of the entrance pupil and  $E'$  the center of the exit pupil.  $\varphi$  and  $\varphi'$  denote the included angles between optical axis and chief ray on the object and image side, respectively. The corresponding angles between marginal ray and optical axis are  $\alpha$  and  $\alpha'$ . (b) Detailed view (dashed box of (a)) of the optical design in the anterior segment. Adapted from [2].

the object height  $h_o$  and  $\varphi = |h_o|/\overline{O_0E}$ , we may thus rewrite (2.1) as

$$|h'_i| = m |h_o| \frac{\overline{E'I'_0}}{\overline{O_0E}}. \quad (2.2)$$

### 2.1.2

#### Cardinal Points

For human eyes, the description of optical imaging can be simplified by introducing three types of *cardinal points*.<sup>8)</sup> In centered optical systems, these points represent special locations on the optical axis which determine the basic imaging properties like image size, image location, and orientation. As the eye is not a centered optical system, we still use the concept of cardinal points but should understand that these points can merely be used as an approximate reference.

**Focal points** When incident light rays cross the object-side focal point  $F$  (Section A.1.2.1) and pass into the eye, they propagate parallel after refraction at cornea and lens. For an emmetropic eye (i.e., without refractive errors; Section 3.1), the image is formed at an infinite distance on the image side. If the incident light rays are parallel, they will be focused on the retina (at point  $F'$ ) after refraction at cornea and (unaccommodated) eye lens.

**Principal points** The two principal points  $P$  and  $P'$  are defined by the intersections of the principal planes (see, e.g., planes  $K$  and  $K'$  in Figure A.8 of Section A.1.2.2) with the optical axis. These points are of interest if the combination of cornea and lens is considered to be one “thick” lens. In this case, the optical design may be simplified by assuming that incident rays are effectively refracted at the two principal planes.

**Nodal points** We consider a light ray emanated from the off-axis object point  $O_1$  in Figure 2.3 which travels towards nodal point  $N$ . After refraction by cornea and lens, the same ray seems to originate from image-side nodal point  $N'$ . The special feature of this ray is that its angle to the optical axis is equal for the ray’s incident (between  $O$  and the corneal front surface) and refracted part (between rear surface of lens and retina). As this ray passes through both nodal points, it is referred to as the *nodal ray*. It also defines the visual axis (Section 2.1.3) of the eye if  $I'_1$  marks the center of the fovea. In centered optical systems, the nodal and chief rays coincide so that the nodal points are actually located in the pupil centers.

**Relation between cardinal points** From geometrical considerations (Figure 2.3), we may derive some useful relations between the cardinal points [2]. We have

$$\mathcal{D}_{\text{eye}} = -\frac{n}{\overline{PF}} = \frac{n'}{\overline{P'F'}} \quad (2.3)$$

$$\overline{PN} = \overline{P'N'} = \frac{n' - n}{\mathcal{D}_{\text{eye}}} \quad (2.4)$$

8) In geometric optics (Appendix A), we also use cardinal points to simplify the description of optical imaging. However, the artificial systems discussed in that chapter are centered so that only focal and principal points must be considered. In decentered optical systems like the human eye, we also have to introduce nodal points.

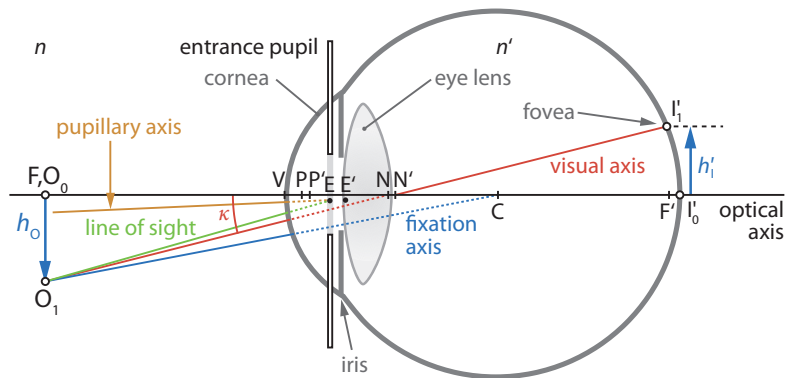


**Figure 2.3** Axes and cardinal points of the eye with corresponding inclination angles.  $V$  is the point of intersection of the optical axis with the cornea (*corneal vertex*).  $E$  and  $E'$  represent the centers of the entrance and exit pupils.  $N$  and  $N'$  denote the nodal points of the eye,

and  $C$  is the rotation center of the eye.  $P$  and  $P'$  are the principal points of the eye.  $n$  and  $n'$  represent the refractive indices outside and inside the eye, and  $\kappa$  is the angle between visual axis and optical axis. Adapted from [2].

$$\overline{FN} = \overline{P'F'} , \tag{2.5}$$

$$\overline{FP} = \overline{N'F'} . \tag{2.6}$$

$\mathcal{D}_{\text{eye}}$  denotes the total refractive power of the human eye,  $n$  is the refractive index of the object space (usually air), and  $n'$  the refractive index of the image space (i.e., the refractive index of the vitreous). Values for  $\mathcal{D}_{\text{eye}}$  and  $n'$  will be specified in Section 2.2.

### 2.1.3

#### Eye Axes

In centered optical systems, the optical axis is usually determined by the line which intersects with the centers of curvature of all refracting and reflecting surfaces. Since the ocular parts are decentered, it is useful to “redefine” the optical axis of an eye as the best-fit line between the centers of curvature of all refracting surfaces (black line in Figure 2.3). In addition, we introduce some other axes that help us to describe the eye’s optical geometry (see also [2]).

**Visual axis** The line between the fixated point  $O_1$  and fovea by way of nodal points  $N$  and  $N'$  is referred to as the *visual axis*. The visual axis thus consists of the two line segments  $\overline{O_1N}$  and  $\overline{N'I'_1}$  (red line in Figure 2.3) and forms the actual imaging axis of the eye. On average, the optical axis and the visual axis enclose an angle of  $\kappa \approx 5^\circ$  on the object side.

With the visual axis, we can once again determine the retinal image size (compare with Section 2.1.1). In the case of paraxial optics, the absolute value of the

retinal image size is given by

$$|h'_1| = \kappa \overline{N'I'_0} \quad (2.7)$$

$$= |h_o| \frac{\overline{N'I'_0}}{\overline{O_0N}}, \quad (2.8)$$

where  $\kappa = -h_o/\overline{O_0N}$ .

**Line of sight** The *line of sight* is given by the line between a fixated object point  $O_1$  and the center of entrance pupil E (green line in Figure 2.3). On average, the angle between the line of sight and the pupillary axis is approximately  $2.5^\circ$ . The position at which the line of sight crosses the cornea is referred to as the *corneal sight center*.

**Pupillary axis** The *pupillary axis* passes through the center of entrance pupil E and is perpendicular to the corneal surface (orange line in Figure 2.3). It is used as an objective measure to judge the amount of eccentric fixation. As the eye is not a centered optical system, the entrance pupil is often not concentric to the cornea. The cornea may also have an irregular shape. Both factors cause the pupillary axis to be different from the optical axis. However, for the following discussions, we assume the center of the entrance pupil to lie on the optical axis.

**Fixation axis** The *fixation axis* is the reference axis for eye movements. It is determined by the line between object point  $O_1$  and center of eye rotation C (blue line in Figure 2.3).

#### 2.1.4

##### Accommodation

In healthy eyes, the refractive power of the eye lens is at maximum  $\mathcal{D}_1 = 20\text{ D}$  and thus contributes only  $\leq 30\%$  to the total eye refraction.<sup>9)</sup> However, within a certain limit, the lens is able to change the refractive power so that nearby as well as distant objects can be sharply imaged on the retina. This process is referred to as *accommodation*. The range over which the refractive power can be changed depends on age.

**Mechanism of accommodation** If the eye focuses on nearby objects, the ciliary muscle is contracted and the zonular fibers are relaxed (*accommodated eye*). When the tension on the lens is decreased, the elasticity of the lens capsule keeps it in a more spherical shape (upper part of Figure 2.4). As the lens becomes more strongly curved in this case,<sup>10)</sup> the eye's total refractive power increases (*near vision*). To focus objects which are located far away from the eye (*far vision*), the deformable, elastic

9) The lower refractive power of the eye lens results from the smaller difference of refractive indices at the aqueous humor–lens and lens–vitreous interfaces.

10) This corresponds to a reduced radius of curvature.

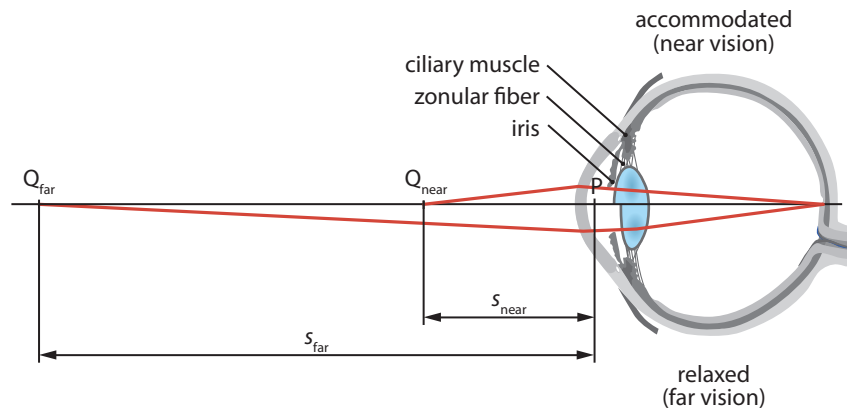


**Figure 2.4** Physiology of accommodation. Upper half of figure: If the ciliary muscle is contracted, the zonular fibers are relaxed and the elasticity of the lens capsule keeps the lens in a more spherical shape. In this case, the refractive power of the lens is higher so that nearby objects can be imaged (near vision). Lower half of figure: To fixate objects which

are located far away from the eye (far vision), the deformable eye lens is brought to an elliptical shape by pulling on the lens capsule. The pulling force which acts on the zonular fibers is generated by a relaxed ciliary muscle. For reference, the near point  $Q_{\text{near}}$ , far point  $Q_{\text{far}}$ , principal point P, and the corresponding distances ( $s_{\text{near}}$  and  $s_{\text{far}}$ ) are shown.

lens is brought to a more elliptical shape by pulling on the lens capsule. The pulling force acting on the zonular fibers is generated by a *relaxed* ciliary muscle (*relaxed eye*). This situation is illustrated in the lower part of Figure 2.4.

Accommodation is an unconscious process that is not yet fully understood. But it is a common belief that chromatic aberrations (Section A.1.9) may deliver the required optical stimulus [3, 4].

**Range of accommodation** The refractive power of the eye lens can be changed only within certain limits. The upper and lower limits of attainable refractive power determine the *range of accommodation* within which sharp vision is possible. The endpoints of the range of accommodation are called *far* and *near point*, respectively. The far point  $Q_{\text{far}}$  is the object point imaged by the eye when the total refractive power is minimal. The near point  $Q_{\text{near}}$  is the object point imaged by the eye when the total refractive power is maximal. The corresponding distances of  $Q_{\text{far}}$  and  $Q_{\text{near}}$  from the object-side principal point P (Section 2.1.2) of the eye are referred to as the *far point distance*  $s_{\text{far}}$  and *near point distance*  $s_{\text{near}}$ , respectively. If  $s_{\text{far}}$  or  $s_{\text{near}}$  are situated in front of the eye, the distances are negative. If they lie (virtually) behind the eye, the distances are set positive. The inverse distances are called the *far point refraction*  $A_{\text{far}} = 1/s_{\text{far}}$  and *near point refraction*  $A_{\text{near}} = 1/s_{\text{near}}$  ( $[A_{\text{far}}] = [A_{\text{near}}] = \text{D}$ ).

The difference between far and near point refraction is referred to as the *amplitude of accommodation*

$$\Delta A_{\text{max}} = A_{\text{far}} - A_{\text{near}} . \quad (2.9)$$

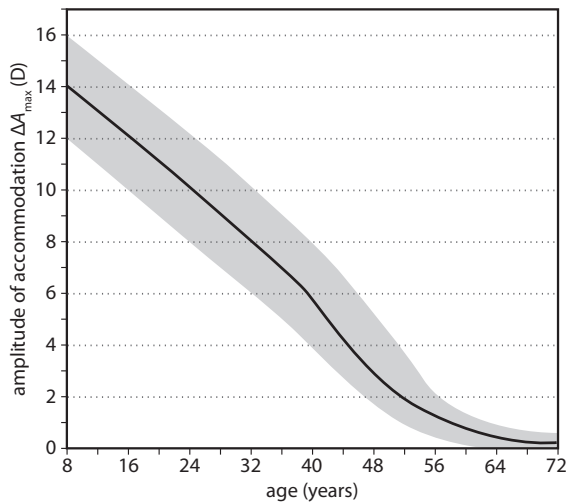


**Figure 2.5** Age-dependence of the amplitude of accommodation  $\Delta A_{\max}$ . The typical range of deviation from the mean values (black curve) is shown in gray. Data taken from [6].

For example, if  $Q_{\text{far}}$  lies at optical “infinity”<sup>11)</sup> ( $A_{\text{far}} = 0$  D) and  $Q_{\text{near}}$  at a distance of  $s_{\text{near}} = 0.2$  m ( $A_{\text{near}} = -5$  D), the amplitude of accommodation is  $\Delta A_{\max} = 5$  D. The amplitude of accommodation is not constant during life. With advancing age, the elasticity of the lens and thus the range of accommodation decreases. As a consequence, humans usually need eye glasses for near vision at the age of 50. This reduction of  $\Delta A_{\max}$  (Figure 2.5), called *presbyopia*, is *not* a refractive error or an eye disease (Chapter 3), but a usual consequence of aging. According to [5], about 1.04 billion people suffered from presbyopia in 2005, 67% of which (696 million people) live in less- and least-developed regions of the world.

### 2.1.5 Resolution

The resolution of an optical system can be defined as the smallest distance between two Airy disks which can be perceived as being separated (Section A.2.1.6). Let us consider the resolution of the human eye by using the same approach. At a wavelength of 550 nm and a pupil diameter of 3 mm, we obtain from (A77) a minimum angle of resolution (MAR) for the eye of  $\theta_{\text{eye,min}} = \text{MAR} = 48''$  (arcsec)  $\approx 1'$  (arcmin). This value merely reveals the normal maximum possible optical resolution of a diffraction-limited eye (Section A.2.1.6). To evaluate the eye’s maximum possible anatomic resolution, we have to consider the photoreceptor spacing as well. In the fovea, the density of cones is maximal (Figure 1.10b), and a nearly one-to-one connection exists between cones and retinal ganglion cells. Cones in the fovea have

<sup>11)</sup> This means that the far point  $Q_{\text{far}}$  is infinitely far away from the eye. An incident bundle of rays emanated from this point is thus parallel (i.e. *collimated light*).

a center-to-center distance of about  $2\ \mu\text{m}$ . When the images of two adjacent point sources stimulate two adjacent cones, they are perceived as being only one point source. If, however, there is one cone unstimulated in between those stimulated by the point sources, then their images are perceived as being separated. As a consequence, a minimum separation of  $\approx 4\ \mu\text{m}$  between image points is required. This value corresponds well to the angle of  $48''$  at the nodal point, taking into account that the image-side nodal point lies about 17 mm in front of the retina (Figure 2.13). The angular limit of photoreceptor resolution is thus in agreement with the minimum angle of resolution of a diffraction-limited eye. In the case of scotopic vision (Section 1.2.1) however, the eye's resolution is much lower ( $\theta_{\text{eye}} > 10'$ ). As the output signal of about 100 rods is combined into one ganglion cell, the effective size of one "detector pixel" is much larger and sensitivity is much higher, too.

### 2.1.5.1 Visual Performance

The values we have calculated for MAR can only be achieved with healthy eyes under ideal ambient light conditions. Normal vision may be impaired by refractive errors (Section 3.1), higher-order aberrations (Section 5.4), eye diseases (Sections 3.2–3.7), and/or problems with the processing of visual signals.

To quantify the visual performance of a patient, we could directly determine the minimum angle of resolution (MAR). In practice, however, this quantity could be a bit confusing, since a large angle means low vision and vice versa. Thus, the visual performance is usually expressed by the inverse of the minimum angle of resolution

$$V = \frac{1}{\text{MAR}}, \quad (2.10)$$

where  $V$  is the so-called *visual acuity*, which we will preferably use in this book. A patient with  $V = 1$  ( $[V] = 1' = (\text{arcmin})^{-1}$ ) is considered to have normal vision. By definition, the visual acuity scale is divided into intervals such that the quotient of two adjacent values of  $V$  is constant<sup>12)</sup> (e.g.,  $1/1'$ ,  $1/1.3'$ ,  $1/1.6'$ ,  $1/2.0'$ ,  $1/2.5'$ ). As a consequence, the visual acuity scale has 22 divisions ranging from  $V = 0.020$  to  $V = 2.5$ . After three scale divisions the visual acuity has doubled.

Another common measure for the visual performance is specified by the common logarithm of the minimum angle of resolution ( $\log_{10} \text{MAR}$ ). This so-called *logMAR* scale is particularly used in scientific publications. The visual acuity scale is related to the logMAR scale via

$$V = 10^{-\log \text{MAR}} \quad (2.11)$$

and can also be defined via distances. As a reference parameter, a distance is chosen at which two object points or lines can be clearly distinguished under an angle of  $1'$ . For example, two points separated by 1.75 mm are placed at a distance of 6 m so that they appear at an angle of  $1'$ . If a test person can perceive these as two points only from a distance of 3 m, then his or her visual acuity is consequently  $V = 0.5$  (which corresponds to  $0.3 \log \text{MAR}$ ).

12) This actually corresponds to a decibel (dB) scale.

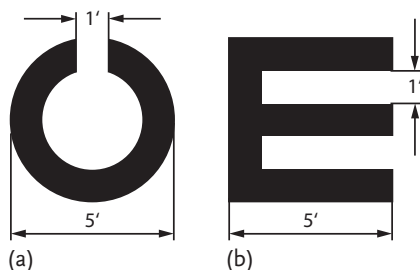


**Figure 2.6** Two typical symbols which are used to determine the visual acuity. For subjective measurements, the symbols are displayed in different sizes and in various states of rotation. The patient then has to state in which direction the respective feature of in-

terest shows. This type of chart can thus also be used for patients who are illiterate or too young to read. (a) Landolt ring. The feature of interest is the gap of the “C”-shaped symbol. (b) Snellen E. The feature of interest is the limb.

### 2.1.5.2 Determination of the Visual Performance

Visual acuity is measured by subjective methods. The smallest feature size which can be clearly resolved by the patient determines the visual acuity. For this purpose, a wall chart with *Landolt rings*<sup>13)</sup> (Figure 2.6a) is used as a test target. The symbols are displayed in different sizes and orientations at a defined distance from the patient. The patient is now asked to state in which direction the corresponding feature of interest shows. The smallest feature which can be clearly recognized by the patient determines the visual acuity. For example, if a patient is able to recognize the orientation of Landolt ring gaps (top, right, bottom, left) with a gap size of 1.75 mm at a distance of 6 m, he or she has a visual acuity of 1. Patients with a lower visual acuity see a blurred image (e.g., the Landolt ring is perceived as a closed ring or dot) and thus cannot find the right feature orientation.

In clinical practice, the so-called *Snellen chart* is used as an alternative measure for the visual acuity. It consists of letters of the alphabet (see e.g. the “Snellen E” in Figure 2.6b) which are arranged in rows. In each row, the size of the letters is different so that each row can be used to test a different level of acuity. The rating of the acuity relates to the distance at which an emmetropic test person (“normal” visual acuity) is able to recognize the letters in that line. The (Snellen) visual acuity is defined by

$$V_S = \frac{\text{testing distance (in m)}}{\text{distance (in m) at which test line letters subtend an angle of } 5'}. \quad (2.12)$$

The 6/6 acuity line represents the “normal” line and contains letters that subtend an angle of 5' (with a minimum feature size of 1') at a distance of 6 m.

Subjective methods do not only check the performance of the pure optical system, but also determine the image processing capability of the sensory organ on the whole (i.e., the combined eye–brain imaging system).

13) Edmund Landolt (1846–1926).

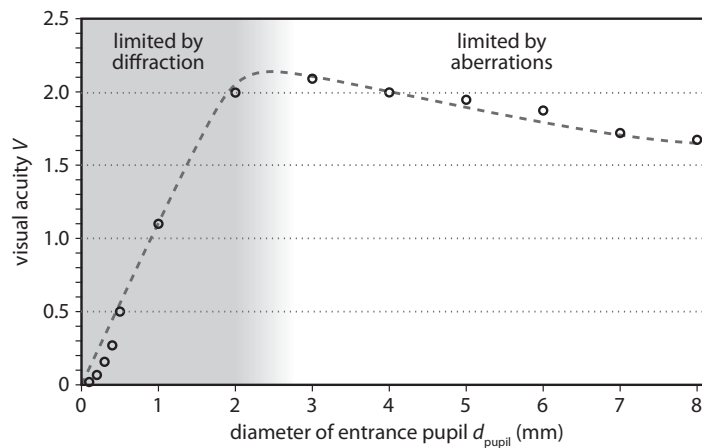


**Figure 2.7** Diameter of the eye's entrance pupil versus visual acuity. A maximum visual acuity is attained for a pupil diameter of about 2.5 mm. Below 2.5 mm (gray area), the optical performance is limited by diffraction. Above 2.5 mm, aberrations deteriorate the optical resolution of the eye. Data points are taken from [7]. The dashed line is a best-fit curve through the data points and meant as a guidance.

### 2.1.5.3 Influence Factors on the Visual Performance

As already mentioned, refractive errors and insufficient ambient light conditions decrease the visual acuity of human eyes. In addition, a number of other factors may influence vision, such as the diameter of the eye's entrance pupil (Figure 2.7). For photopic vision (Section 2.1.6), the best resolution is given for a pupil diameter of about  $d_{\text{pupil}} \approx 2.5$  mm. A smaller pupil diameter deteriorates the resolution as diffraction (Section A.2.1.6) comes into play. If the pupil diameter is larger, optical aberrations (Section A.1.6) reduce the resolution so that the visual acuity eventually "saturates".

As the density of cones and ganglion cells rapidly decreases outside the fovea, the visual performance for photopic vision also depends on the field angle at which the image is projected on the retina (Figure 2.8). At the optic nerve head, no photoreceptors exist at all so that the visual acuity equals to zero in this area (the so-called blind spot). Other influence factors for the visual performance are the shape, brightness, and color of considered objects as well as the degree of attention (psychological influence factors).

### 2.1.6

#### Adaption

The eye is able to maintain a high sensitivity to small changes in light intensity across a broad range of ambient light levels. Full operation of human vision is possible for a luminance between  $10^{-6}$  and  $10^8$  cd/m<sup>2</sup> [8]. For this purpose, the eye uses the following mechanisms to adapt to the given ambient light conditions:

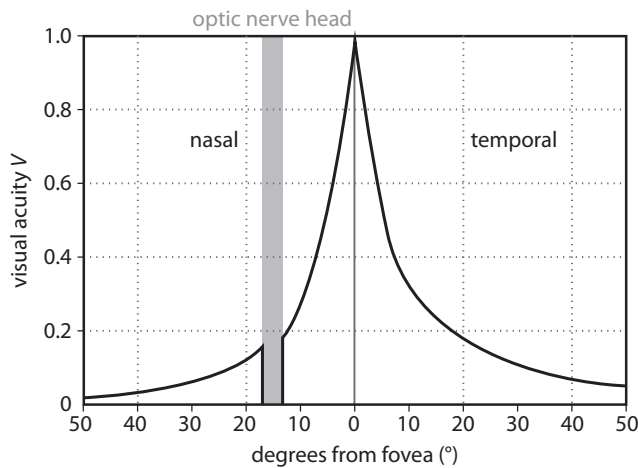


**Figure 2.8** Dependence of the visual acuity on the field angle for photopic vision. The density of cones is maximal at the fovea ( $0^\circ$ ), but rapidly decreases outside this retinal region. As a consequence, the resolution is gradually reduced for increasing field angles. Adapted from [6].

1. As discussed in Section 1.2, the retina has two types of photoreceptors (rods and cones), which are used at different illumination levels. The operational range of rods – which ends at rod saturation – spans a remarkable 8 orders of magnitude in luminance (Figure 2.9). In the range of *scotopic vision*, only rods are used. Cones operate even over a range of 11 orders of magnitude in luminance, at which the range of operation partly overlaps with the rods (*mesopic vision*). If the luminance is higher than  $10 \text{ cd/m}^2$ , only cones are used for vision (*photopic vision*). The “operational” range of each type of photoreceptor can be regulated by biochemical (Section 1.2.1) and neuronal processes in the pigments within the outer segment (Figure 1.9). Since these processes are relatively slow, the adaption of the photoreceptors takes several minutes. Therefore, a faster adaption process is required which protects the retina from overload and damage.
2. The inner diameter of the iris diaphragm can be changed by the so-called *pupil reflex*<sup>14)</sup>. This mechanism is the first stage of sensitivity regulation when the ambient light level is changed. When the iris diameter reduces from 8 mm (maximum diameter at total darkness) to 2 mm (minimum diameter at very high light levels), the area of the aperture stop decreases by a factor of 16. As a consequence, the iris can regulate the amount of light which enters the eye only by one order of magnitude. This is obviously not sufficient to account for the manageable luminance range of 14 orders of magnitude. The variation of the iris diameter is thus only responsible for the first stages of adaption, before the photoreceptors adjust their sensitivity according to the present luminance.

14) The term “pupil” can be misleading. In optics, the hole in the iris acts as an aperture stop. Only the image of this hole formed by the cornea should be referred to as a “pupil”.

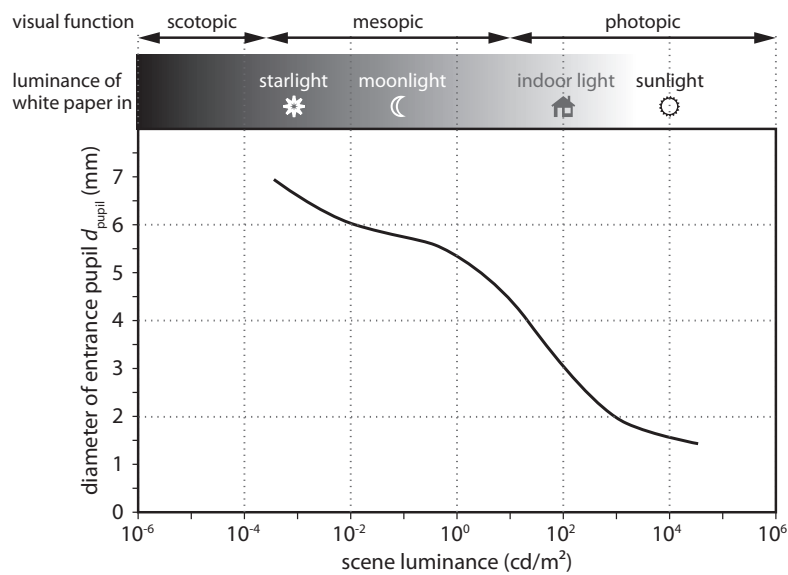


**Figure 2.9** Range of illumination levels which can be handled by the eye. The luminance magnitudes of a white paper in starlight, in moonlight, indoors, and in sunlight are also shown for reference. Data taken from [9].

Let us consider the process when the ambient light level becomes low (transition from photopic to scotopic vision). As discussed, the inner diameter of the iris increases, the rods are activated, and the brain starts to increase the neural detection time of the photoreceptors. The adaption process to darkness takes about 40 min to complete. During the first 7 min, new pigments are generated for the cones so that the threshold sensitivity for the smallest detectable visual stimulus is increased by a factor of 50. During the following 30 min, the rod pigment rhodopsin is produced which increases the sensitivity of the retina by a factor of 1000 [6]. At low light levels, the sensitivity is high, but the spatial resolution of the eye is reduced (Section 2.1.5) and colors cannot be distinguished (Section 2.3).

In the reverse case of high ambient light conditions (photopic vision), the iris diameter decreases, the cones are activated, and the neural detection time is reduced. As a consequence, the eye is no longer sensitive to small changes in light intensity. The biochemical adaption of cones takes about 3–4 min. The spatial resolution and the color perception is enhanced compared to scotopic vision.

### 2.1.7

#### Stiles–Crawford Effect

Due to the tapered shape of cones (Figure 1.9), incident light is guided towards the end of the photoreceptors by total internal reflection (Section A.1.1), similar to an optical waveguide (Section 10.2.4.2). Light rays which pass through the center of the eye's entrance pupil are incident at a small angle to the cones of the curved

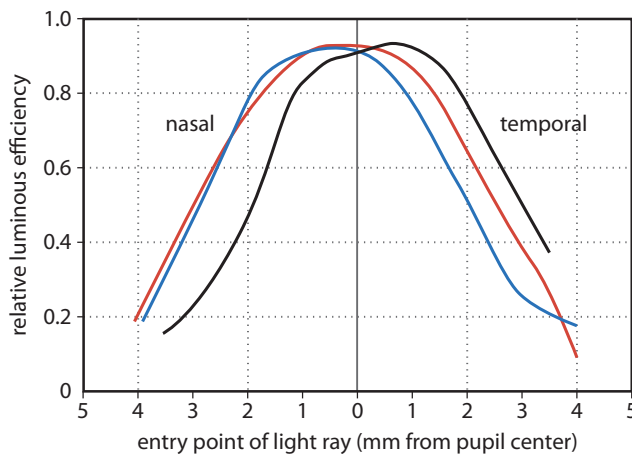


**Figure 2.10** The relative luminous efficiency of a focused target versus the horizontal pupillary position of the beam. The values were measured under photopic conditions for three test persons (different curve colors). Apparently, the maximum efficiency is not measured in the center of the entrance pupil. Data taken from [8].

retina and stimulate the cones more “effectively” than rays which pass through the outer zone of the pupil. If the angle of incidence is large, the total reflection is suppressed and not all rays can be absorbed. This phenomenon is referred to as the *Stiles–Crawford effect*. The relative luminous efficiency, that is, the amount of light which is detected by the photoreceptors versus the incident luminance, is shown for three different test persons in Figure 2.10. We see that the effect varies slightly for every person and is not always symmetric about the center of the entrance pupil. However, a simple function to fit the data in Figure 2.10 can be given by [8]

$$\log_{10} \left( \frac{\eta_{SC}}{\eta_{SC,max}} \right) \approx -0.07 r^2, \quad (2.13)$$

where  $\eta_{SC}/\eta_{SC,max}$  is the relative luminous efficiency and  $r$  the distance of the ray from the pupil center. The Stiles–Crawford effect has a positive effect on the image quality of the eye, because the influence of spherical aberration (Section A.1.6.1) decreases for a large pupil diameter.

### 2.1.8

#### Depth of Field

If an object is moved slightly away from the focal point, this has only a little effect on the quality of the retinal image. But the image quality deteriorates progressively as we move further away from the focal point. The depth of field  $\Delta z_{dof}$  is defined as the maximum distance the object can be shifted and the image still reveals an acceptable sharpness.  $\Delta z_{dof}$  depends on the state of adaption (Section 2.1.6) and is affected by retinal, neural, and psychophysical factors. A commonly used empirical

formula to determine the depth of field for the human eye is given by [10]

$$\Delta z_{\text{dof}} = \frac{\lambda}{2\text{NA}^2} + \frac{1}{7\text{NA}\beta}, \quad (2.14)$$

where  $\lambda$  denotes the wavelength of the incident light and NA the numerical aperture (Section A.1.4) of the eye.  $\beta$  is the magnification (Section A.1.2.1) of the eye that depends on the state of accommodation. Similar to camera systems, a large diameter of the aperture stop – which corresponds to a high NA – thus means a small depth of field. In (2.14), accommodation was taken into account by ways of  $\beta$ .

### 2.1.9

#### Binocular Vision

Both eyes are arranged in a common plane and separated by an *interpupillary distance* PD (i.e., the distance between both pupil centers) of 50–75 mm. This special arrangement allows humans to get a three-dimensional impression of the environment. For example, we can estimate depth and distance of objects which are placed in a row. This property of binocular vision is referred to as *stereopsis*. It is based on the comparison of two slightly different retinal images by the brain. In more concrete terms, both images received by the eyes are two-dimensional but horizontally shifted. The brain is now able to combine this information to “generate” a three-dimensional image and can distinguish between any objects which are located in different planes along the viewing direction (i.e., the  $z$  direction in Figure 2.11).

Figure 2.11 shows a top-view scene of two eyes of a person who fixates object point  $O_{\text{fix}}$ .  $O_{\text{fix}}$  is located at a distance  $L$  from the nodal plane<sup>15)</sup> of the eyes (Section 2.1.3) and is sharply imaged onto each fovea. Object point  $O_f$ , which lies in front of  $O_{\text{fix}}$ , is imaged onto the temporal sides of both eyes (image point  $I'_f$ ). Object point  $O_b$ , which lies behind  $O_{\text{fix}}$ , is imaged onto the nasal sides of the eyes (image point  $I'_b$ ). The retinal images of  $O_b$  are closer together than the images of  $O_f$  which is “translated” to a different position in depth.

In Figure 2.11, the temporal ray of the right eye crosses the nasal ray of the left eye at point A. Similarly, the temporal ray of the left eye crosses the nasal ray of the right eye at point B. Points A and B are both located on the object plane and separated by the *parallax* distance  $s_p$  with which we can write the *stereo angle* as

$$\varepsilon = 2 \arctan\left(\frac{s_p}{2L}\right). \quad (2.15)$$

The minimum stereo angle determines the smallest angle that can be resolved by the eye and still allows stereoscopic perception. Under appropriate conditions, the human eye has a minimum stereo angle of  $\varepsilon_{\text{min}} = 10''$  [6].

A related quantity is the stereoscopic depth perception  $\Delta L$  [12]. This quantity specifies the distance between two objects in a row which can be perceived as being

15) At the nodal point (Section 2.1.3), the incident light rays are crossing the optical axis of an eye. The nodal points of both eyes lie on one common *nodal plane*.



human eye can be calculated as

$$\Delta L_{\min} = \frac{\varepsilon_{\min} s_{\text{nv}}^2}{\text{PD}} = 45 \mu\text{m} . \quad (2.19)$$

With adequate visual aids (e.g., surgical microscopes; Section 6.2),  $\Delta L_{\min}$  can be further reduced. For this purpose, we can either enlarge the *stereo base* (i.e., the effective interpupillary distance), e.g., by mirrors or prisms, or increase the magnification of the image so that the three-dimensional image impression is considerably enhanced. Without visual aids, stereopsis breaks down at object distances  $> 500 \text{ m}$ .

Besides stereopsis, limited depth perception of distant objects can be attained with just one eye as well. In this case, the distinction in depth is based on recognition patterns and experience. Some typical determining factors are:

- recognition of perspective, that is, smaller objects appear to be further away than larger objects,
- partial overlap of objects,
- distribution of light and shadows, and
- parallax of motion, that is, a moving object appears to be slower if it is further away.

#### 2.1.10

##### Spectral Properties

Since water is the major substance of the eye's optical components, the spectral properties (Figure 9.3) such as absorption and scattering are determined by those of water.<sup>16)</sup> In particular for wavelengths  $\lambda > 600 \text{ nm}$ , the absorption of water dominates the spectral properties of ocular media. For wavelengths  $\lambda < 600 \text{ nm}$ , however, proteins and chromophores become important.

Figure 2.12 shows the transmittance spectrum at different locations in the eye. We can see that wavelengths below 400 nm and above 1400 nm are totally absorbed by the eye's ocular media, whereas the transmittance remains higher than 0.6 in the spectral range between 420 and 920 nm (see transmittance at retina (black) in Figure 2.12).

With regard to dispersion, the properties of ocular media are determined by the Abbe number (see Eq. (A6))  $\nu_{\text{eye}} \approx 50.2$ . Hence, eye tissue shows a higher degree of dispersion than most silica glasses.

<sup>16)</sup> This is certainly true for the aqueous humor. In cornea and lens, proteins are included so that the absorption properties are slightly different for them. Nevertheless, it is reasonable to model the spectral properties of an eye by a water depth of 16 mm.

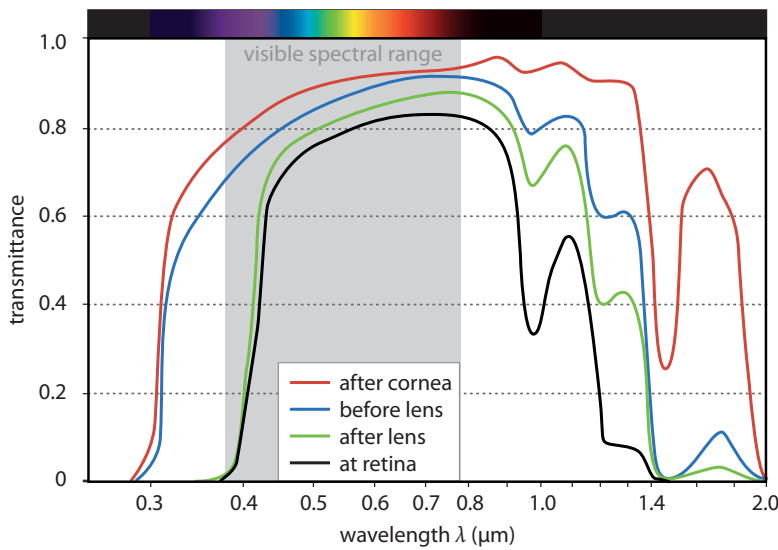


**Figure 2.12** Spectral transmittance inside the eye after the incident light has passed the cornea (red), the aqueous humor (blue), the lens (green), and the vitreous (black). The

wavelength scale is not linear. For reference, a color bar is added at the top of the diagram. Data taken from [6].

## 2.2 Schematic Eye Models

Both the optical properties and the geometry of eyes that we have discussed so far vary between human beings. This obviously makes it difficult to design and simulate optical devices where the eye is part of the whole system – regardless of whether the eye acts as a detector or as the examined object. To deal with this issue in a somewhat more rigorous manner, schematic *eye models* [2] have been developed which emulate real eyes under certain boundary conditions as closely as possible. The eye parameters included in the eye models are basically average values that have been determined from measurements on many test eyes. Depending on the intended applicative situation (relaxed eye, accommodated eye; Section 2.1.4), we can utilize more or less accurate and complicated eye models<sup>17)</sup>. In this context, we distinguish between *paraxial models* (Section 2.2.1), which are only valid in the case of paraxial approximation, and *finite wide-angle models* (Section 2.2.2), which are also able to describe aberrations (Sections A.1.6–A.1.9) quantitatively.

17) An eye model is called *exact* if it includes at least four refracting surfaces, i.e., two corneal and two lenticular surfaces.

2.2.1

**Paraxial Model: The Gullstrand Eye**

In optometry, the most common paraxial eye model is the *Exact Gullstrand<sup>18)</sup> Eye #1*, which is based on measured data from accommodated and relaxed eyes<sup>19)</sup>. Consequently, two versions of this model exist for different states of accommodation of the eye lens:<sup>20)</sup> 0 D and 10.878 D.

**2.2.1.1 Optical Properties**

In the Exact Gullstrand Eye, we assume the refracting surfaces to be spherical and centered at a common optical axis. Since all ocular media of the model have a constant refractive index, the refractive power of the lens is varied by implementing a lens core (central nucleus) of high refractive index which is surrounded by an outer shell (cortex) with lower refractive index. All in all, the Exact Gullstrand Eye thus consists of six (i.e., two corneal and four lenticular) refracting surfaces (Figure 2.13). The geometric and optical parameters for the relaxed and accommodated state are listed in Table 2.1.

In the Exact Gullstrand Eye, the total refractive power of the cornea  $\mathcal{D}'_c$  can be calculated with the *Gullstrand formula* (or *thick lens formula*)

$$\mathcal{D}'_c = \mathcal{D}'_a + \mathcal{D}'_p - \frac{L_c}{n_c} \mathcal{D}'_a \mathcal{D}'_p. \tag{2.20}$$

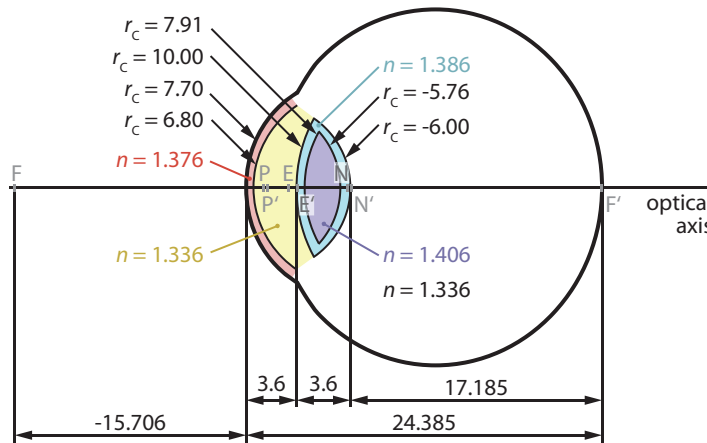


**Figure 2.13** Scheme (2 : 1 scale) of the Exact Gullstrand Eye #1 for relaxed vision based on data from Table 2.1. The radii of curvature and lengths are given in millimeters.

18) Alvar Gullstrand (1862–1930).

19) Other paraxial eye models are discussed in-depth in [2, 6].

20) The original version of the Exact Gullstrand Eye cannot be used to model variable accommodation. However, with some modifications, continuous accommodation may be included [2].

**Table 2.1** Parameters of the Exact Gullstrand Eye #1 for relaxed (0 D accommodation) and accommodated vision (10.878 D accommodation). The locations refer to the vertex of the cornea (point V in Figure 2.3).  $r_C$  denotes the radius of curvature,  $L$  is the thickness, and  $n$  the refractive index of the respective eye component. Data taken from [2, 13].

Parameter	Relaxed vision	Accommodated vision	
Location of object-side focal point F (mm)	-15.706	-12.397	
Location of image-side focal point F' (mm)	24.385	21.016	
Location of object-side nodal point N (mm)	7.078	6.533	
Location of image-side nodal point N' (mm)	7.331	6.847	
Location of object-side principal point P (mm)	1.348	1.772	
Location of image-side principal point P' (mm)	1.601	2.086	
Location of entrance pupil E (mm)	3.047	2.668	
Diameter of entrance pupil (mm)	8.000	8.000	
Location of exit pupil E' (mm)	3.665	3.212	
Diameter of exit pupil (mm)	7.276	7.524	
Refractive power of cornea (D)	43.053	43.053	
Refractive power of lens (D)	19.111	33.057	
Refractive power of eye (D)	58.636	70.576	
Total eye length (mm)	24.385	24.385	

	Relaxed vision			Accommodated vision		
	$r_C$ (mm)	$L$ (mm)	$n$	$r_C$ (mm)	$L$ (mm)	$n$
Corneal front surface	7.700	-	-	7.700	-	-
Cornea	-	0.500	1.376	-	0.500	1.376
Corneal back surface	6.800	-	-	6.800	-	-
Anterior chamber	-	3.100	1.336	-	2.700	1.336
Front surface of lens cortex	10.000	-	-	5.333	-	-
Anterior lens cortex	-	0.546	1.386	-	0.673	1.386
Front surface of lens core	7.911	-	-	2.655	-	-
Lens core	-	2.419	1.406	-	2.655	1.406
Back surface of lens core	-5.760	-	-	-2.655	-	-
Posterior lens cortex	-	0.635	1.386	-	0.673	1.386
Back surface of lens cortex	-6.000	-	-	-5.333	-	-
Vitreous	-	17.185	1.336	-	17.185	1.336

$\mathcal{D}'_a$  denotes the refractive power of the corneal front surface (air–cornea interface) and  $\mathcal{D}'_p$  the refractive power of the corneal back surface (interface between cornea and anterior chamber).  $n_c$  and  $L_c$  are the refractive index and the thickness of the cornea, respectively. In optometry, one often uses the *corneal back vertex power*  $\mathcal{D}'_{cv}$  instead of  $\mathcal{D}'_c$ .  $\mathcal{D}'_{cv}$  represents the inverse distance from the corneal back vertex to

its image-side focus and is given by [13]

$$\mathcal{D}'_{cv} = \frac{\mathcal{D}'_c}{1 - L_c \mathcal{D}'_a / n_c} . \quad (2.21)$$

In paraxial approximation, the refractive power of a spherical surface (also referred to as the *surface power*)<sup>21)</sup> is determined by

$$\mathcal{D}' = \frac{n' - n}{r_c} , \quad (2.22)$$

where  $n$  and  $n'$  are the refractive indices of the media on the incident and the refracted side, respectively. Equation (2.22) corresponds to the right side of (A11) in Section A.1.2 for which we now use the dioptric equivalents.

Let us now apply (2.20)–(2.22) to the Exact Gullstrand Eye model. With the values from Table 2.1, we obtain

$$\mathcal{D}'_a = \left( \frac{1.376 - 1}{0.0077} \right) D = 48.83 \text{ D} , \quad (2.23)$$

$$\mathcal{D}'_p = \left( \frac{1.336 - 1.376}{0.0068} \right) D = -5.88 \text{ D} . \quad (2.24)$$

With (2.20), the total refractive power of the cornea follows as

$$\mathcal{D}'_c = \left( 48.83 - 5.88 - \frac{0.0005}{1.336} \cdot 48.83 \cdot (-5.88) \right) D = 43.06 \text{ D} , \quad (2.25)$$

and for the corneal back vertex power, we obtain  $\mathcal{D}'_{cv} = 43.86 \text{ D}$ .

For many applications, the Exact Gullstrand Eye is still too “complicated”. In these cases, it is possible to simplify the model without introducing noticeable errors. In the so-called *Simplified Gullstrand Eye #1* (Table 2.2), the cornea is represented by a single refracting surface. In this simplified model, the lens has just two refracting surfaces instead of four.

### 2.2.1.2 Treatment of Aberrations

In the first instance, the Gullstrand Eye model is meant to adequately describe the optics of the human eye only for paraxial rays. In real eyes, we also have to deal with nonparaxial or obliquely incident rays which are affected by optical aberrations (Section A.1.5). For example, the pupil diameter allows oblique rays to be projected onto the retina, and the ocular media show considerable dispersion. Refractive errors and diseases (Chapter 3) intensify the naturally given aberrations even further. In the following, we examine if, and to what extent, the Gullstrand Eye can “handle” optical aberrations.

21) The surface power quantifies the ability of the lens surface to change the direction of an incident light ray, i.e., the degree of divergence or convergence.

**Table 2.2** Parameters of the Simplified Gullstrand Eye #1 for relaxed (0 D accommodation) and accommodated vision (8.599 D accommodation). The locations refer to the vertex of the cornea.  $r_C$  denotes the radius of curvature,  $L$  is the thickness, and  $n$  the refractive index of the respective eye component. Data taken from [13].

Parameter	Relaxed vision	Accommodated vision	
Location of object-side focal point F (mm)	-14.983	-12.561	
Location of image-side focal point F' (mm)	23.896	21.252	
Location of object-side nodal point N (mm)	7.062	6.562	
Location of image-side nodal point N' (mm)	7.363	6.909	
Location of object-side principal point P (mm)	1.550	1.782	
Location of image-side principal point P' (mm)	1.851	2.128	
Location of entrance pupil E (mm)	3.052	2.674	
Diameter of entrance pupil (mm)	8.000	8.000	
Location of exit pupil E' (mm)	3.687	3.249	
Diameter of exit pupil (mm)	7.334	7.532	
Refractive power of cornea (D)	42.735	42.735	
Refractive power of lens (D)	21.755	32.295	
Refractive power of eye (D)	60.483	69.721	
Total eye length (mm)	23.896	23.896	

	Relaxed vision			Accommodated vision		
	$r_C$ (mm)	$L$ (mm)	$n$	$r_C$ (mm)	$L$ (mm)	$n$
Corneal front surface	7.800	-	-	7.800	-	-
Anterior chamber	-	3.600	1.333	-	3.200	1.333
Front surface of eye lens	10.000	-	-	5.000	-	-
Eye lens	-	3.600	1.416	-	4.000	1.416
Back surface of eye lens	-6.000	-	-	-5.000	-	-
Vitreous	-	16.696	1.333	-	16.696	1.333

**Spherical aberration** In the Gullstrand Eye model, 60% of the total spherical aberration (Section A.1.6.1) is caused by the anterior corneal surface and 30% by the posterior surface of the lens. The accommodated Gullstrand Eye shows  $3 \times$  more spherical aberration than the relaxed version. Interestingly, real eyes have much less spherical aberration than calculated from the paraxial model. For example, the spherical aberration of the Gullstrand Eye is  $6 \times$  higher than corresponding experiments have shown for light rays entering the pupil at a ray height of 4 mm (Figure 2.16).

**Astigmatism** For real eyes, astigmatism (Section A.1.6.3) occurs when the eye's refractive parts are irregular (Section 3.1.2) or in the case of obliquely incident rays. Compared to real eyes, the Gullstrand Eye shows more astigmatism for oblique

rays. For example, we have a deviation by a factor of 2 when the light rays are incident at angles  $< 50^\circ$ .

**Field curvature** Because of the curved shape of the retina, the field curvature (Section A.1.6.4) has nearly no influence on imaging. We can understand this by looking at Figure A.19 in Section A.1.6.4. In the eye, the image surface is curved so that the incident off-axis rays are focused on the retina. Up to an angle of incidence of  $30^\circ$ , this behavior is well reproduced by the Gullstrand Eye. For angles  $> 30^\circ$ , field curvature is still irrelevant for real eyes, whereas it becomes important for the Gullstrand Eye.

**Distortion** Distortion (Section A.1.6.5) mainly depends on both position and diameter of the entrance pupil. With regard to distortion, the Gullstrand model predicts the imaging behavior of real eyes quite well.

**Chromatic aberration** As dispersion (Section A.1.1) is not included to the Gullstrand model, chromatic aberration (Section A.1.9) cannot be modeled. Nevertheless, chromatic effects play an important role for the imaging with real eyes.

In summary, the Gullstrand Eye model is *not* able to describe aberrations caused by nonparaxial rays with sufficient accuracy. In addition, chromatic aberrations are not considered at all. It is thus useful to develop more sophisticated schematic eye models which are able to describe nonparaxial optics and dispersion as well.

## 2.2.2

### Finite Wide-Angle Models

Paraxial eye models can be further improved when we try to reproduce the optical and geometric parameters of real eyes as exactly as possible. For example, we may include the facts that the surfaces of cornea and lens are not spherical (aspheric lenses) and that the refracting surfaces are not centered at a common axis. We can also add dispersion to the models and/or describe the lens with a gradient refractive index, instead of the shell approach used for the Exact Gullstrand Eye. But we have to bear in mind that every generalization increases the complexity of the model, which makes calculations even more challenging. In the following, we present two prominent examples for so-called *finite wide-angle models* which allow the description of the imaging of human eyes for nonparaxial rays and off-axis object points quite well.

#### 2.2.2.1 Navarro Eye Model

In the Navarro Eye model (Figure 2.14), the refractive parts of the eye are represented by four aspheric surfaces (so-called *conicoids*) which are centered to a common optical axis. Each surface is determined by the condition

$$x^2 + y^2 + (1 + Q)z^2 - r_C z = 0, \quad (2.26)$$

**Table 2.3** Parameters of the Navarro Eye. The locations refer to the vertex of the cornea.  $A$  is the state of accommodation in diopters (D).  $r_C$  denotes the radius of curvature,  $L$  is the thickness, and  $Q$  the asphericity parameter of the respective eye component.  $n$  is the re-

fractive index for a wavelength of 589.3 nm. The additional parameters  $r_{C3}$ ,  $r_{C4}$ ,  $L_2$ ,  $L_3$ ,  $n_3$ ,  $Q_3$ , and  $Q_4$  depend on the state of accommodation and are defined in the text. Data taken from [2, 6, 14].

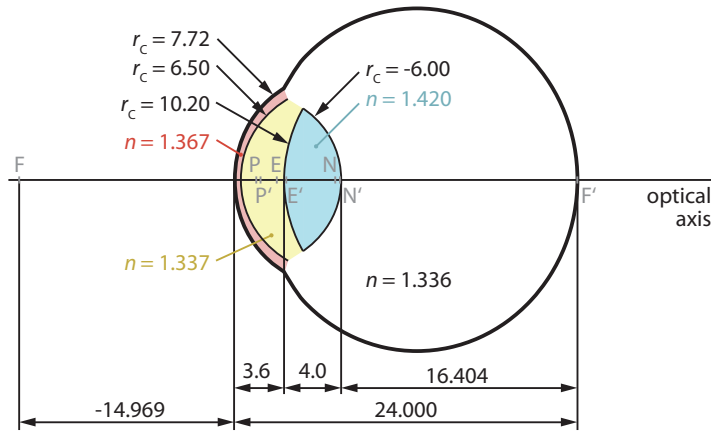
Parameter	Relaxed vision ( $A = 0$ D)	Accommodated vision ( $A = 10$ D)
Location of object-side focal point F (mm)	-14.969	-12.051
Location of image-side focal point F' (mm)	24.004	21.172
Location of object-side nodal point N (mm)	7.145	6.727
Location of image-side nodal point N' (mm)	7.452	7.116
Location of object-side principal point P (mm)	1.583	2.005
Location of image-side principal point P' (mm)	1.890	2.393
Location of entrance pupil E (mm)	3.042	2.928
Location of exit pupil E' (mm)	3.682	3.551
Refractive power of cornea (D)	42.882	42.882
Refractive power of lens (D)	21.779	34.548
Refractive power of eye (D)	60.416	71.145
Total eye length (mm)	24.004	24.000

	$r_C$ (mm)	$L$ (mm)	$n$	$Q$
Corneal front surface	7.72	-	-	-
Cornea	-	0.55	1.3670	-0.2600
Corneal back surface	6.50	-	-	-
Anterior chamber	-	$3.05 - L_2$	1.3374	0
Front surface of eye lens	$10.20 - r_{C3}$	-	-	-
Eye lens	-	$4.00 + L_3$	$1.4200 + n_3$	$-3.1316 - Q_3$
Back surface of eye lens	$-6.00 + r_{C4}$	-	-	-
Vitreous	-	16.403 98	1.3360	$-1.000 - Q_4$

where  $r_C$  denotes the radius of curvature,  $Q$  the asphericity parameter, and  $z$  the direction of the optical axis. The refractive index of the eye lens is assumed to be constant for a given wavelength. Analogous to other models, all optical and geometric parameters are based on average data taken from measurements. The corresponding data set is listed in Table 2.3.

Accommodation is fully included in the Navarro Eye model in that the distance between cornea and lens as well as the lens parameters are functions of the state of accommodation. As a consequence, some parameters in Table 2.3 have additional terms which depend on the state of accommodation  $A$  (in D), that is,



**Figure 2.14** Scheme (2 : 1 scale) of the Navarro Eye for relaxed vision based on data from Table 2.3. The radii of curvature and lengths are given in millimeters.

$$r_{C3} = 1.75 \ln(A + 1) ,$$

$$r_{C4} = 0.2294 \ln(A + 1) ,$$

$$L_2 = 0.05 \ln(A + 1) ,$$

$$L_3 = 0.1 \ln(A + 1) ,$$

$$n_3 = 9 \times 10^{-5} (10A + A^2) ,$$

$$Q_3 = 0.34 \ln(A + 1) ,$$

$$Q_4 = 0.125 \ln(A + 1) .$$

In contrast to the Gullstrand Eye model, chromatic dispersion is fully included in the Navarro Eye (see [14]). For this purpose, the ocular media are described by the so-called *Herzberger formula* which is given by

$$n(\lambda) = a_1(\lambda)n^{**}(\lambda = 365\text{nm}) + a_2(\lambda)n_F(\lambda = 486.1\text{ nm}) + a_3(\lambda)n_c(\lambda = 656.3\text{nm}) + a_4(\lambda)n^*(\lambda = 1014\text{ nm}) . \quad (2.27)$$

The coefficients are determined by

$$a_1(\lambda) = 0.661\,471\,96 - 0.040\,352\,796 \mu\text{m}^{-2} \lambda^2 - \frac{0.280\,467\,9 \mu\text{m}^2}{\lambda^2 - \lambda_0^2} + \frac{0.033\,859\,79 \mu\text{m}^4}{(\lambda^2 - \lambda_0^2)^2} , \quad (2.28)$$

$$a_2(\lambda) = -4.201\,463\,83 + 2.735\,089\,56 \mu\text{m}^{-2} \lambda^2 + \frac{1.505\,437\,84 \mu\text{m}^2}{\lambda^2 - \lambda_0^2} - \frac{0.115\,932\,35 \mu\text{m}^4}{(\lambda^2 - \lambda_0^2)^2} , \quad (2.29)$$

**Table 2.4** Refractive indices of ocular media used in the Herzberger formula (2.27). Data taken from [14].

Ocular Medium	$n^{**}$ ( $\lambda = 365 \text{ nm}$ )	$n_F$ ( $\lambda = 486.1 \text{ nm}$ )	$n_c$ ( $\lambda = 656.3 \text{ nm}$ )	$n^*$ ( $\lambda = 1014 \text{ nm}$ )
Cornea	1.3975	1.3807	1.37405	1.3668
Aqueous humor	1.3593	1.3422	1.3354	1.3278
Lens	1.4492	1.42625	1.4175	1.4097
Vitreous	1.3565	1.3407	1.3341	1.3273

$$a_3(\lambda) = 6.298\,342\,37 - 4.694\,099\,35 \mu\text{m}^{-2} \lambda^2 - \frac{1.575\,086\,5 \mu\text{m}^2}{\lambda^2 - \lambda_0^2} + \frac{0.102\,930\,38 \mu\text{m}^4}{(\lambda^2 - \lambda_0^2)^2}, \quad (2.30)$$

$$a_4(\lambda) = 1.758\,350\,59 + 2.362\,537\,94 \mu\text{m}^{-2} \lambda^2 + \frac{0.350\,116\,57 \mu\text{m}^2}{\lambda^2 - \lambda_0^2} - \frac{0.020\,857\,82 \mu\text{m}^4}{(\lambda^2 - \lambda_0^2)^2}, \quad (2.31)$$

with  $\lambda_0^2 = 0.028 \mu\text{m}^2$  and  $[\lambda] = \mu\text{m}$ . The refractive indices of the ocular media used in Eq. (2.27) for the various optical components are listed in Table 2.4.

#### 2.2.2.2 Liou–Brennan Eye Model

The Liou–Brennan Eye model (geometry shown in Figure 2.15) reproduces the eye geometry fairly exactly. The optical and geometric parameters are based on measurements of people at the ages of about 45. For example, this model can be used advantageously to simulate the visual performance before and after a refractive surgery (Chapter 10).

In the Liou–Brennan Eye, the decentration of the real human eye is also regarded. The corresponding visual axis (red line in Figure 2.15) includes an angle of  $\kappa = 5^\circ$  with the optical axis. The iris is modeled as a circular aperture stop at the front surface of the lens whose center is shifted by 0.5 mm from the optical axis in the nasal direction. Accommodation is, however, not included and parameters are only given for the relaxed eye. Dispersion of the ocular media is set to the dispersion of water, which is approximately

$$n_{\text{water}} \approx 1.3847 - 0.1455 \mu\text{m}^{-1} \cdot \lambda + 0.0961 \mu\text{m}^{-2} \cdot \lambda^2 \quad (2.32)$$

with the wavelength of light  $\lambda$  ( $[\lambda] = \mu\text{m}$ ). Similar to the Navarro Eye, the anterior corneal surface and the surfaces of the eye lens are aspheric. In addition, the eye lens has a gradient refractive index. The distribution of the refractive index at the front surface of the lens (Figure 2.15) is given by

$$n_A(\rho, z) = 1.368 + 0.049\,057 \mu\text{m}^{-1} z - 0.015\,427 \mu\text{m}^{-2} z^2 - 0.001\,978 \mu\text{m}^{-2} \rho^2. \quad (2.33)$$

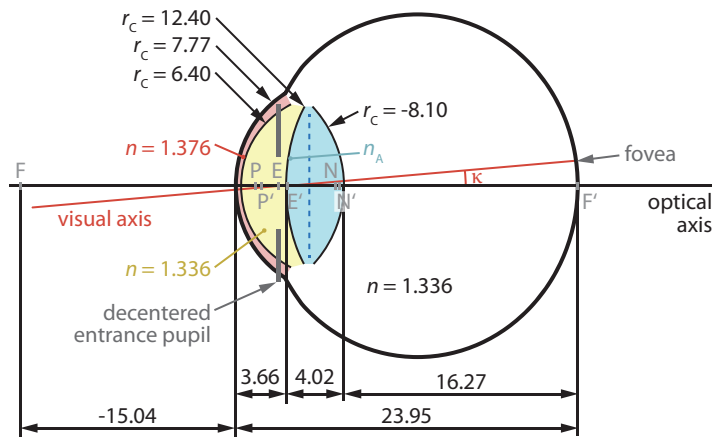


**Figure 2.15** Scheme (2:1 scale) of the relaxed Liou–Brennan Eye model. The radii of curvature and lengths are given in millimeters. The geometry, the visual axis, and the decentration of the entrance pupil (by 0.5 mm nasally) are shown. The blue dashed line represents the lens center, which is an imaginary plane separating the eye lens into anterior and posterior segments.

$\rho = \sqrt{x^2 + y^2}$  ( $[\rho] = \mu\text{m}$ ) is the coordinate normal to the traveling direction  $z$  of the incident light rays. At the central lens surface (dashed blue line in Figure 2.15), the distribution of the refractive index is determined by

$$n_P(\rho, z) = 1.407 - 0.006\,605\,\mu\text{m}^{-2}z^2 - 0.001\,978\,\mu\text{m}^{-2}\rho^2 \quad (2.34)$$

with  $[z] = [\rho] = \mu\text{m}$ .

### 2.2.2.3 Aberrations in Finite Wide-Angle Models

Finite wide-angle models are more realistic than paraxial models. Thus, we expect that the aberrations calculated by finite wide-angle models come closer to experimental data.

**Spherical aberration** In Figure 2.16, the distance of incident light rays at the pupil from the optical axis (ray height) is plotted versus the spherical aberration in diopters (D) for the Gullstrand Eye #1, the Navarro Eye, and the Liou–Brennan Eye. When the calculations are compared with experimental data (circles), we can clearly observe that the finite wide-angle models deliver much better results than the paraxial model. In particular, the Liou–Brennan Eye perfectly matches the experiment.

**Astigmatism** At angles of incidence  $< 50^\circ$ , the Navarro Eye deviates by a factor of  $< 1.5$  from real eyes. Thus, it fits slightly better to experimental data than the paraxial Gullstrand Eye. The Liou–Brennan Eye shows roughly the same behaviour at larger angles as the Navarro Eye, but the deviations from real eyes at small angles of incidence are not as large as for the Navarro Eye.

**Table 2.5** Parameters of the Liou–Brennan Eye. The locations refer to the vertex of the cornea.  $r_C$  denotes the radius of curvature,  $L$  is the thickness, and  $Q$  the asphericity parameter of the respective eye component.  $n$  is

the refractive index at a wavelength of 555 nm.  $n_A$  and  $n_P$  are gradient-index distributions of the unaccommodated lens (see Eqs. (2.33) and (2.34)). Data taken from [2, 15].

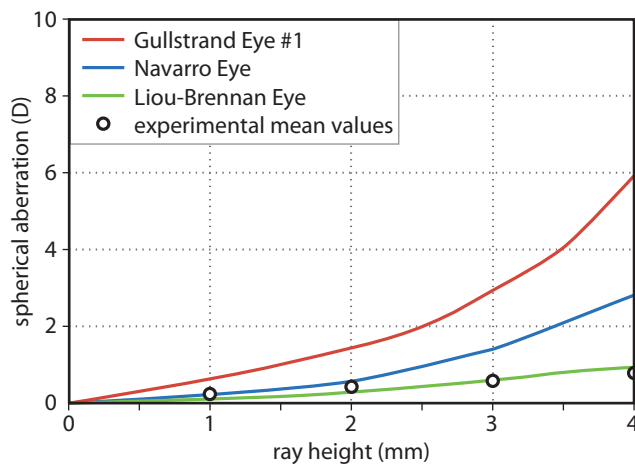
Parameter	Relaxed Vision			
Location of object-side focal point F (mm)	−15.040			
Location of image-side focal point F' (mm)	23.950			
Location of object-side nodal point N (mm)	7.100			
Location of image-side nodal point N' (mm)	7.378			
Location of object-side principal point P (mm)	1.532			
Location of image-side principal point P' (mm)	1.890			
Location of entrance pupil E (mm)	3.098			
Location of exit pupil E' (mm)	3.720			
Refractive power of cornea (D)	42.262			
Refractive power of lens (D)	22.134			
Refractive power of eye (D)	60.314			
Total eye length (mm)	23.950			

	$r_C$ (mm)	$L$ (mm)	$n$	$Q$
Corneal front surface	7.77	–	–	–
Cornea	–	0.50	1.376	−0.18
Corneal back surface	6.40	–	–	–
Anterior chamber	–	3.16	1.336	−0.60
Front surface of eye lens	12.40	–	–	–
Eye lens (front segment)	–	1.59	$n_A$	−0.94
Lens center (dashed line Figure 2.15)	$\infty$	2.43	$n_P$	–
Back surface of eye lens	−8.10	–	–	–
Vitreous	–	16.27	1.336	0.96

**Field curvature** Like for the paraxial Gullstrand Eye, the discussed finite wide-angle models fit exactly to experimental data for small angles ( $< 30^\circ$ ). The finite wide-angle models tend to emulate the field curvature of real eyes better for angles  $> 30^\circ$ .

**Chromatic aberration** Since dispersion is included in both finite wide-angle models, chromatic aberrations can be described by these models quantitatively. The dispersion model of the Navarro Eye was chosen especially with the objective to reproduce experimental data as accurately as possible.



**Figure 2.16** Ray height versus spherical aberration for different eye models. Experimental data points are shown for reference. Regarding spherical aberration, the Liou–Brennan Eye can emulate real eyes very well. Data taken from [2].

### 2.2.3

#### Applications of Eye Models

The optics of the human eye must often be considered for the design of ophthalmic, optometric, and other optical systems. For this purpose, the presented schematic eye models are used to derive the standard optical properties like the refractive powers, the imaging behavior, the positions of cardinal points, the influence of aberrations, and so on. From this, some typical examples for the application of eye models follow:

- Design of corrective glasses and contact lenses
- Design and layout of optical imaging systems and visual aids such as loupes (Section 6.1) and surgical microscopes (Section 6.2)
- Design and layout of diagnostic devices (Chapter 5)
- Simulation and planning of surgeries for treatment of eye diseases and refractive errors (Chapter 10)
- Calculation of derived eye parameters (see Example 2.1).

#### Example 2.1

**Calculation of the Retinal Image Size** As a simple example for the application of eye models, we calculate the retinal image size of a Landolt ring with a height of  $h_O = 6$  mm. We assume that the test person looks at this symbol from a distance of  $L = 4$  m. For the calculation, we use (2.7), as the angle  $\kappa$  of the nodal ray (Figure 2.3) does not change after passage through the eye's refractive parts (Section 2.1.3).<sup>22)</sup>

The angle at which the Landolt ring appears to the test person is given by

$$\kappa = \arctan\left(\frac{h_0}{L}\right) = 5.157' = 0.0015 \text{ rad} . \quad (2.35)$$

The distance between the image-side nodal point  $N'$  and the retinal image surface (represented by image point  $I'_0$ ) can, for example, be taken from the Exact Gullstrand Eye (Table 2.1) for which  $\overline{N'I'_0} = 17.054 \text{ mm}$ . As a consequence, we obtain for the retinal image size

$$h'_1 = \kappa \overline{N'I'_0} = 25.6 \text{ } \mu\text{m} . \quad (2.36)$$

Note that we inserted the value of angle  $\kappa$  in radiant units. The gap feature of the Landolt ring is  $5 \times$  smaller than the whole Landolt ring symbol. On the retina, the gap thus forms an image height of  $5.1 \text{ } \mu\text{m}$ .

When we use the parameters of the Navarro Eye (Table 2.3) instead of the Exact Gullstrand Eye model, the distance between image-side nodal point and retinal image changes to  $\overline{N'I'_0} = 16.548 \text{ mm}$ . Hence, in this case, we obtain a retinal image size of  $h'_1 = 24.8 \text{ } \mu\text{m}$ .

### 2.3 Color Vision

As mentioned in Section 1.2.1, the color perception of eyes mainly depends on the ambient light conditions. For scotopic vision, only rods are used. Rods have a maximum sensitivity at a wavelength of  $507 \text{ nm}$  (black curve in Figure 2.17). This is the reason why we cannot distinguish colors at night.

For photopic vision, the human eye uses three types of cones ( $S$ ,  $M$ ,  $L$  cones) with different spectral sensitivity (Figure 2.17). The three detector types allow us to have *trichromatic vision*. Light with wavelengths between  $380$  and  $780 \text{ nm}$  can be processed by the retina, which actually determines the *visible spectrum*. From the mean value of the sensitivity curves of all cones in Figure 2.17, we obtain a maximum sensitivity at a wavelength of  $555 \text{ nm}$  under photopic conditions.

For vision, the signals of  $S$ ,  $M$ , and  $L$  cones are combined in the brain, resulting in a visual stimulus interpreted as a *color*.<sup>22)</sup> Hence, the color at which an object appears to us is *not* an inherent property of the object itself, but rather depends on

22) In principle, we could also use relation (2.1) to calculate the retinal image size. However, the angle  $\varphi$  of the chief ray is modified by cornea and eye lens (Figure 2.2), and  $\varphi'$  cannot be measured in practice.

23) An unknown number of women may perceive millions of colors invisible to the rest of human beings. It is supposed that they possess 4 (instead of 3) different types of cones which expand the perceivable spectral range [16].

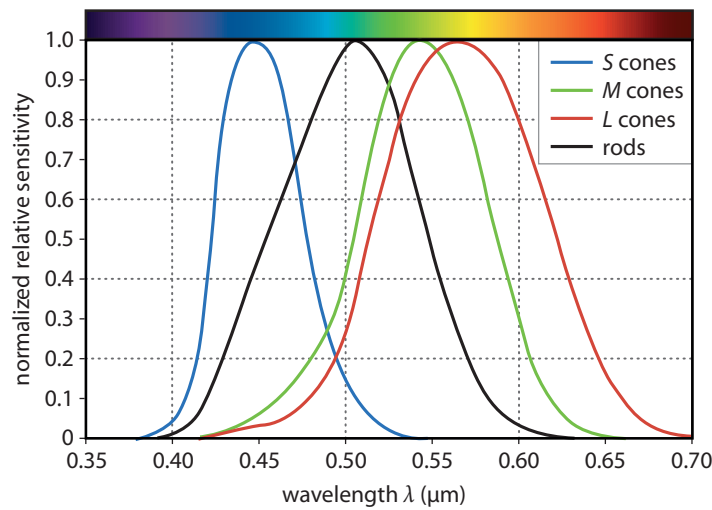


**Figure 2.17** Dependence of normalized relative sensitivity of S, M, L cones, and rods on the wavelength. Data taken from [6].

our visual impression. The wavelength-dependent visual stimulus is characterized by three parameters:

1. *Hue*: The hue determines the degree to which a visual stimulus can be described as similar or different from stimuli described as “red”, “yellow”, and “blue” (i.e., primary hues). It depends largely on what eye and brain perceive to be the predominant wavelength of light reflected or sent from an object.
2. *Saturation*: The saturation characterizes the purity or “richness” of a color. If all the light which is seen by the eye has the same wavelength, the color will appear fully saturated. The more wavelengths are added, the paler (desaturated) the color appears.
3. *Brightness*: The brightness determines the intensity level at which the visual impression is perceived. It is our subjective interpretation of luminance (Section A.2.1.5).

White, gray, and black stimuli cannot be described as a color, as they have no hue and saturation and are completely determined by the brightness.

In contrast to the ear – which is able to distinguish several acoustic frequencies playing at once – the eyes and the brain cannot determine which wavelengths of light are simultaneously present in the observed color. For example, if we look at a monochromatic laser beam which only consist of light with a wavelength of 590 nm, the eye perceives a yellow color. The same impression can be obtained when we spatially overlap two laser beams with wavelengths of 540 and 680 nm and proper intensity. In this case, we do *not* realize that the beam consists of green and red light. This is, in fact, the basis for the concept of primary hues (red, yellow,

blue). With these hues, we can “mix” any other color of the visible spectrum<sup>24)</sup>, for example, cyan is a combination of blue and green.

The full theory of color vision and color formation is beyond the scope of this book. Please refer to references [17–19] for further details about this topic.

## 2.4 Recommended Reading

Further information about the optics of the human eye can be found in standard ophthalmology textbooks, for example, [2, 6, 11, 13].

### References

- 1 Porter, J., Queener, H., Lin, J., Thorn, K., and Awwal, A.A.S. (eds) (2006) *Adaptive Optics for Vision Science: Principles, Practices, Design and Applications*, John Wiley & Sons, Inc, Hoboken.
- 2 Atchison, D.A. and Smith, G. (2006) *Optics of the Human Eye*, Butterworth-Heinemann.
- 3 Aggarwala, K.R., Nowbatsing, S., and Kruger, P.B. (1995) Accommodation to monochromatic and white-light targets. *Invest. Ophthalmol. Vis. Sci.*, **36**, 2695–2705.
- 4 Graef, K. and Schaeffel, F. (2012) Control of accommodation by longitudinal chromatic aberration and blue cones. *J. Vis.*, **12**, 1–12.
- 5 Holden, B.A., Fricke, T.R., Ho, S.M., Wong, R., Schlenker, G., Cronjé, S., Burnett, A., Papas, E., Naidoo, K.S., and Frick, K.D. (2008) Global vision impairment due to uncorrected presbyopia. *Arch. Ophthalmol.*, **126**, 1731–1739.
- 6 Gross, H., Blechinger, F., and Achnert, B. (2008) *Handbook of Optical Systems – Survey of Optical Instruments*, vol. 4, Wiley-VCH Verlag GmbH, Weinheim.
- 7 Holladay, J.T., Lynn, M.J., Waring, G.O., Gemmill, M., Keehn, G.C., and Fielding, B. (1991) The relationship of visual acuity, refractive error, and pupil size after radial keratotomy. *Arch. Ophthalmol.*, **109**, 70–76.
- 8 Optical Society of America (ed.) (1994) *Handbook of Optics: Fundamentals, Techniques, and Design*, vol. 1, McGraw-Hill Professional.
- 9 Tasman, W. (ed.) (1992) *Duane’s Foundations of Clinical Ophthalmology*, vol. 2, Lippincott Williams & Wilkins.
- 10 Gross, H., Zügge, H., Peschka, M., and Blechinger, F. (2007) *Handbook of Optical Systems – Correction of Optical Systems*, vol. 3, Wiley-VCH Verlag GmbH, Weinheim.
- 11 Diepes, H. (2004) *Refraktionsbestimmung*, DOZ Verlag Optische Fachveröffentlichungen GmbH, 3rd edn.
- 12 Schober, H. (1964) *Das Sehen*, vol. 1, VEB Fachbuchverlag Leipzig.
- 13 Smith, G. and Atchison, D.A. (1997) *The Eye and Visual Optical Instruments*, Cambridge University Press.
- 14 Navarro, R., Santamaría, J., and Bescós, J. (1985) Accommodation-dependent model of the human eye with aspherics. *J. Opt. Soc. Am. A*, **2**, 1273–1281.
- 15 Liou, H.L. and Brennan, N.A. (1997) Anatomically accurate, finite model eye

24) As the optical resolution of human eyes is limited, colors can also be generated by additive color composition. This means that the color impression is generated by superposition of small areas (e.g., tiny dots) with primary hues. The hue we perceive is then determined by the relative intensity of each color component. This principle of “composite” colors is, e.g., used for digital image projection and color raster prints.

48 | 2 Optics of the Human Eye

- for optical modeling. *J. Opt. Soc. Am. A*, **14**, 1684–1695.
- 16** Greenwood, V. (2012) The humans with super human vision. <http://discovermagazine.com/2012/jul-aug/06-humans-with-super-human-vision> (accessed 24 August 2013).
- 17** Gross, H. (2005) *Handbook of Optical Systems – Fundamentals of Technical Optics*, vol. 1, Wiley-VCH Verlag GmbH, Weinheim.
- 18** Still, D., Fletcher, R. (eds) (1998) *Eye Examination and Refraction*, Wiley-VCH Verlag GmbH, Weinheim.
- 19** Valberg, A. (2005) *Light Vision Color*, Wiley-VCH Verlag GmbH, Weinheim.